Trends in surface radiation and cloud radiative effect at four Swiss sites for the 1996 – 2015 period

Stephan Nyeki[1], Stefan Wacker[2], Christine Aebi[1,3], Julian Gröbner[1], Giovanni Martucci[4], and Laurent Vuilleumier[4]

[1] Physikalisch-Meteorologisches Observatorium/World Radiation Center, Davos, Switzerland.
[2] Deutscher Wetterdienst, Meteorologisches Observatorium Lindenberg/Richard-Aßmann-Observatorium, Lindenberg, Germany.
[3] Oeschger Center for Climate Change Research and Institute of Applied Physics, University of Bern, Bern, Switzerland.
[4] Federal Office of Meteorology and Climatology MeteoSwiss, Payerne, Switzerland.

Correspondence to: Stephan Nyeki (stephan.nyeki@pmodwrc.ch)

Abstract. The trends of meteorological parameters and surface downward shortwave and longwave radiation (DSR, DLR) were analyzed at four stations (between 370 and 3580 m asl) in Switzerland for the 1996 – 2015 period. Ground temperature, specific humidity and atmospheric integrated water vapor (IWV) increased during all-sky and cloud-free conditions. All-sky DSR and DLR trends were in the ranges 0.6 – 4.3 W m^{-2}/decade and 0.9 – 4.3 W m^{-2}/decade, respectively, while corresponding cloud-free trends were -2.9 – 3.3 W m^{-2}/decade and 2.9 – 5.4 W m^{-2}/decade. The cloud radiative effect (CRE) was determined using radiative transfer calculations for cloud-free DSR and an empirical scheme for cloud-free DLR. CRE decreased in magnitude by 0.9 – 3.1 W m^{-2}/decade which implies a reduction in cloud cover and/or a change towards a different cloud type over the four Swiss sites. Between 10 and 70% of the increase in DLR is explained by factors other than ground temperature and IWV. Trends in aerosol optical depth at each station over the same period remained insignificant, and thus their contribution to the observed changes in surface radiative fluxes was negligible. A more detailed, long-term quantification of cloud changes is crucial and will be possible in the future as cloud cameras have been measuring at three of the four stations since 2013.

1 Introduction

Downward shortwave and longwave radiation (DSR, DLR) are important terms in the surface radiation budget and are fundamental in understanding the climate effect of increasing greenhouse gas concentrations (Wang and Dickinson, 2013). Both DSR and DLR have been reliably and accurately monitored since the late 1980s/early 1990s in several ground-based networks including: i) the Baseline Surface Radiation Network (BSRN) (Ohmura et al., 1998; König-Langlo et al., 2013), ii) the Atmospheric Radiation Measurement (ARM) program (Ackerman and Stokes, 2003), and iii) the Surface Radiation (SURFRAD) Network (Augustine et al., 2000). DSR over Europe was observed to decrease in the 1950s to 1980s ("dimming"), and was followed by an increase ("brightening") to the present which has been attributed to changes in cloud cover and/or aerosol concentrations (e.g. Wild, 2009; Wang and Dickinson, 2013; Wild, 2016a; and references therein). DLR has also been observed to increase (Wang and Liang, 2009; Wild, 2016b), although the reliable observational record is only several decades long at present.

In support of these international efforts, the Alpine Surface Radiation Budget (ASRB) network was established in 1994/1995 at eight stations in Switzerland to monitor regional radiation fluxes (Philipona et al., 1996; Marty, 2000; Marty et al., 2002). In a trend analysis of the 1995 – 2002 DLR time series at these stations it was observed that average DLR increased by 5.2 and 4.2 W m^{-2} for all-sky and cloud-free conditions, respectively (Philipona et al., 2004). A later study found an average cloud-free increase of 3.5 W m^{-2} for the 1996 – 2007 period at four of these stations (Wacker et al., 2011) which were still in operation.

It was estimated that >50% of the DLR trend was due to the positive trends in temperature and humidity. However, clouds can

also significantly modify the radiation budget by reflecting shortwave and emitting longwave radiation. In order to quantify this with respect to the radiation budget, the concept of a Cloud Radiative Effect (CRE) can be used which is the difference between all-sky radiation fluxes and cloud-free simulated fluxes (Ramanathan et al., 1989). Trends in the CRE at the same four Swiss stations were observed by Wacker et al. (2011) to decrease by up to 7.5 W m^{-2}, indicating a reduction in the

5   fractional cloud cover (FCC) or a change towards a different cloud type.

This study presents an update of radiation fluxes for the 1996 – 2015 period, spanning 20 continuous years of surface radiation measurements at each of the four Swiss stations. Our objectives are: i) to assess whether trends in all-sky and cloud-free surface radiation can be determined and explained with any greater certainty, ii) to assess the trends in the shortwave and longwave CRE, and iii) apply a wider range of robust statistical techniques than in previous studies.

2 Methods

2.1 Data from ASRB and SACRaM Networks

The ASRB network monitored DSR and DLR at eight existing stations belonging to the Swiss Federal Institute of Meteorology (MeteoSwiss) from 1992 to 1995. Measurements were conducted according to BSRN guidelines. In a subsequent rationalization of the network, only four of the original eight stations continued to operate. These included (in order of altitude):

15   Locarno (LOC, 46.180°N, 8.783°E, 367 m), Payerne, (PAY, 46.815°N, 6.944°E, 491 m), Davos (DAV, 46.814°N, 9.846°E, 1594 m asl), and Jungfraujoch (JFJ, 46.549°N, 7.986°E, 3580 m). Instruments from these stations were incorporated into the MeteoSwiss CHARM (Swiss Atmospheric Radiation Monitoring) network which were then merged in the 2007 – 2012 period to a single network, the Swiss Alpine Climate and Radiation Monitoring network (SACRaM). Several aspects concerning the instruments are worth noting and are therefore briefly discussed here:

i) Pyrgeometers in the ASRB network were all unshaded, and hence a correction was applied using the method described by Dürr (2004). In contrast, DLR data from the SACRaM network are not corrected. However, the PIR pyrgeometers are either shaded or CG(R)4 pyrgeometers are used instead which are less affected by heating effects or by longwave irradiance in the direct beam of the sun (Meloni et al., 2012; Gröbner et al., 2018).

25

ii) The SACRaM data acquisition systems were updated in stages from March 2005 to October 2011 which resulted in several short monitoring gaps. For instance, monitoring at PAY was interrupted from August 23, 2011 to November 1, 2011, but was not considered to be long enough to affect the trend analysis in this study.

30   iii) SACRaM radiometers at DAV are located at and maintained by the Physikalisch-Meteorologisches Observatorium Davos/World Radiation Center (PMOD/WRC). Due to major building renovation from December 2010 to September 2012, these radiometers were partially removed from December 2010 to December 2014, however, PMOD/WRC radiometers were re-located nearby. DSR data from the SACRaM network was available while DLR data from the World Infrared Standard Group (WISG) of pyrgeometers (WMO, 2006) was used for the January 2006 to December 2015 period instead. The WISG

35   consists of four pyrgeometers, which were averaged into a single DLR time series of 1-min data.

iv) The PMOD/WRC hosts the World Standard Group (WSG) of pyrheliometers and the WISG, as mentioned above. These provide the reference scales for shortwave and longwave radiation measurements, respectively. However, several studies have determined that their reference scales may need to be revised in the future (Fehlmann et al., 2012; Gröbner et al., 2014). The

40   WSG scale overestimates by 0.3%, and a straightforward linear correction can be applied. However, the WISG scale underestimates longwave fluxes which will require a non-linear correction depending on a number of factors (e.g. raw signal

data, etc.) reported by Gröbner et al. (2014) and Nyeki et al. (2017). The latter study determined that corrections lay in the ranges ~1 – 4 W m^{-2} for all-sky DLR and ~5 – 7 W m^{-2} for cloud-free DLR when based on available data from four BSRN stations having the longest time series. A correction of the SACRaM DSR time series should have no effect on the trend analyses in this study while a correction of DLR time series may marginally affect the trends depending on the degree of

5   cloudiness at each station. While such corrections are beyond the scope of the present study, they should be kept in mind when future comparisons are made.

v) The uncertainty of pyranometer measurements is estimated to be in the range 18 – 23 W m^{-2} (Vuilleumier et al., 2014). Similarly, the uncertainty of pyrgeometer measurements is estimated at ±4 W m^{-2}, and their relative stability is within ±1 W m^{-2}

10   over extended time periods (Gröbner et al., 2014; Nyeki et al., 2017).

vi) Meteorological data (10-min resolution), integrated water vapor (IWV; 1-min resolution) from Global Navigation Satellite System (GNSS) measurements (Morland et al., 2006) (STARTWAVE database, www.startwave.ch), and DSR and DLR data (1-min resolution) were available as quality controlled and assured data from MeteoSwiss. Monthly average values were then

15   constructed for time series analysis. Use of a method by Roesch et al. (2011) to construct monthly averages was considered, which minimizes the risk of biased monthly mean values when calculated from incomplete or flagged data records of DSR and DLR. A comparison of results for all sky conditions with simple monthly averages gave results which were different by <0.1%. Cloud-free time series could not be constructed with this method due to the frequent cloud cover at all stations. Hence, for the sake of consistency and comparability, simple monthly averages were used throughout this study for the trend analyses.

20   A monthly average was accepted for all-sky conditions if ≥75% of data were available for each month.

2.2 Cloud-Free Conditions

In order to calculate cloud-free climatologies of meteorological parameters and radiation fluxes, the occurrence of cloud-free conditions needs to be determined. The first method uses 10-minute measurements of screen-level temperature at 2 m above ground (T_{2m}), relative humidity and DLR as input data to a semi-empirical algorithm, the Automatic Partial Cloud Amount

25   Detection Algorithm (APCADA) (Dürr and Philipona, 2004). The degree of cloudiness, can be derived in oktas (0 to 8) and then converted to FCC (1 okta = 0.125 FCC) for any 10-minute period during any time of the day. Cloud-free versus cloudy cases can be distinguished with an uncertainty of about 5% for low to mid-level clouds. APCADA has the advantage that night-time FCC data can be derived for the four locations in this study based on previous semi-empirical studies (e.g. Dürr and Philipona, 2004). APCADA has several minor drawbacks. The first one is a difficulty in adequately detecting high-altitude

30   clouds (particularly optically thin cirrus) because of their low radiative impact at the surface. However, as the radiative effect of such clouds on DLR is small, the effect of cloud contamination in the cloud-free dataset is considered to be small. The second drawback is that APCADA semi-empirical calibration values (lapse rate coefficient and effective cloud-free broadband emissivity) are based on climatological conditions at each location in the early 1990s. While these calibration values are not expected to have changed since then, this cannot be verified here without an updated analysis. An alternative method, presented

35   by Long and Turner (2008), determines the cloud cover using meteorological parameters and various statistical thresholds based on current data. It was argued that clear-sky estimates were more accurate, but a comparison with APCADA remains to be conducted in a future study.

The second method to determine the degree of cloud cover uses visible sky cameras. Although FCC is only available during the daytime and only since 2013, it was used here to assess whether it could help to refine the APCADA method. Sky cameras

40   were installed at PAY (VIS-J1006, Schreder GmbH) and at DAV (Q24M, Mobotix). A camera was also installed at JFJ but image overexposure meant that reliable data was not available. Images taken at PAY have a temporal resolution of five minutes, and two are sequentially taken with different exposure times (1/500 and 1/1600 s) having a 1200 x 1600 pixel resolution. One

image is taken each minute at Davos with an exposure time of 1/500 s. After the pre-processing of images (Aebi et al., 2017), a color ratio (the sum of the blue to green ratio plus the blue to red ratio) is calculated per pixel (Wacker et al., 2015) and compared to a reference value (2.2 in Davos and 2.5 in Payerne). A pixel is classified as being cloudy or cloud-free based on this comparison. The FCC is then calculated by summing up the cloudy pixels and dividing by the total number of pixels. FCC

5   values ≤0.05 for each 10 min value were attributed to cloud-free conditions which is more stringent than for APCADA where the limit is ≤ 1 okta (i.e. FCC ≤ 0.125).

2.3 Parameterization of Cloud-Free DSR and DLR

As mentioned in Section 1, the effect of clouds on the surface radiation budget can be expressed by the CRE (Eq. 1) which is divided into components for the shortwave and longwave cloud effects (SCE and LCE, respectively). Each component itself

10   is defined as the difference between all-sky fluxes (e.g. $DSR_{all-sky}$) and corresponding simulated cloud-free conditions (e.g. $DSR_{sim\,cloud-free}$), as in Eq. 2:

$$CRE = SCE + LCE,\qquad\qquad\qquad (1)$$

15   $$CRE = DSR_{all-sky} - DSR_{sim\,cloud-free} + DLR_{all-sky} - DLR_{sim\,cloud-free},\qquad\qquad (2)$$

CRE is defined here using just the downward flux components, similar to other studies (e.g. McFarlane et al., 2012), rather than the net (i.e. downward – upward) fluxes (e.g. Berg et al., 2011), so care must be taken when comparisons are made. $DSR_{sim\,cloud-free}$ in Eq. 2 was calculated using the solar zenith angle, IWV, and aerosol optical depth (AOD) as inputs to

20   libRadtran (Library for Radiative Transfer) (Mayer and Kylling, 2005). AOD was derived using procedures and data published previously (Nyeki et al., 2012; Kazadzis et al., 2018), and was only available for 1994 – 2013. Climatological averages from this period were used to construct AOD for the missing period, 2013 – 2015. $DLR_{sim\,cloud-free}$ was calculated using the empirical parameterization by Prata (1996) as in Eq. 3:

25   $$DLR_{sim\,cloud-free} = (1 - (1 + w).exp(-(1.2 + 3.w)^{0.5})).\,\sigma T^4_{2m},\qquad\qquad (3)$$

Where T_{2m} is in Kelvin, σ is the Stefan-Boltzmann constant (5.67×10^{-8} W m^{-2} K^{-4}), e is the water vapor pressure (hPa), and $w = 46.5e/T_{2m}$. As w is in fact the parameterization for IWV (in cm), observed values of IWV from GNSS measurements were used instead. A modified form of the above Prata parameterization was developed by Gröbner et al. (2009) by using the

30   effective atmospheric boundary layer temperature instead of T_{2m}. This temperature modification as well as use of the Prata parameterization was considered by Wacker et al. (2014) to be slightly more accurate than the modified Brutsaert parameterization used by Wacker et al. (2011). The former was therefore used as the main parameterization of $DLR_{sim\,cloud-free}$ in this study. In a validation study of various $DLR_{sim\,cloud-free}$ models using the 1996 – 2008 time series from the same four Swiss SACRaM stations, Gubler et al. (2012) noted that a well-adapted and validated parameterization was in fact more important

35   than the type of parameterization itself.

An alternative parameterization of $DLR_{sim\,cloud-free}$, reported by Ruckstuhl et al. (2007), was briefly investigated as well. Also using data from the same four Swiss SACRaM stations, Ruckstuhl et al. (2007) parameterized $DLR_{sim\,cloud-free}$ with GNSS-derived IWV. A power-law of the following form was found for this DLR-IWV parameterization when data from all four stations was combined:

40

$$\text{DLR} = a.\text{IWV}^b , \tag{4}$$

where the coefficients a and b were calculated for cloud-free conditions. It was determined that observed and parameterized monthly values for the 2001 – 2004 period gave correlation coefficients $R^2 > 0.95$ and had root-mean-square errors (rmse) of

5   9.2 – 12.0 W m^{-2}. It was concluded that $\text{DLR}_{\text{sim cloud-free}}$ could be parameterized with an uncertainty of <5% when based on monthly average values. The main reason for including this method here, is to test whether $\text{DLR}_{\text{sim cloud-free}}$ can be more accurately parameterized with longer IWV time series than in previous studies (Ruckstuhl et al., 2007) in order to calculate LCE. This method was also used to test Eq. 4 during all-sky and not just cloud-free conditions. A temperature modification could not be applied as only IWV appears in Eq. 4.

10   **2.4 Statistical Methods**

Trend analyses were performed using several methods. The first was the linear least squares (LLS) method by Weatherhead et al. (1998), using de-seasonalized monthly average values. Further details are given in the forerunner study by Wacker et al. (2011). The second method uses the seasonal Kendall test and Sen's slope estimator (see Gilbert, 1987; and references therein). The seasonal Kendall test is an extension of the Mann-Kendall test, a non-parametric technique which determines whether a

15   monotonic increasing or decreasing trend exists. The test takes seasonal effects into account and hence avoids the problem of auto-correlation in the time series. In order to check the homogeneity of the time series, three statistical tests were applied: the Buishand test (parametric), the Pettitt test (non-parametric), and the standard normal homogeneity test (SNHT; parametric) (Wijngaard et al., 2003). The null hypothesis is that the values of the testing variable are independent and identically distributed, while a stepwise change in the mean (or other statistic) is present under the alternative hypothesis. When correctly

20   used, these tests can locate when a possible change occurred. The SNHT test is more sensitive to changes near the beginning and end of a time series, whereas the Buishand and the Pettitt tests are more sensitive to changes in the middle. In order to meet the normality assumption for the SNHT and Buishand tests, monthly time series were log-transformed.

3 Results and Discussion

3.1 Meteorological and Surface Radiation Climatologies

25   Tables 1 and 2 summarize meteorological and radiation flux statistics for all-sky and cloud-free climatologies, respectively, at all four stations. Seasonal averages (DJF, MAM, etc.) clearly illustrate an annual cycle in virtually all parameters with a maximum in summer and minimum in winter. All-sky values in Table 1, not previously reported, are similar to cloud-free values in Table 2 for the 1996 – 2007 period reported by Wacker et al. (2011). T_{2m} and DSR values are seen to be slightly lower in Table 1, as would be expected during cloudy conditions. In contrast, the specific humidity and IWV are higher during

30   all-sky conditions which in turn results in higher DLR values. For a number of reasons, IWV at JFJ was based on a widely-used parameterization using T_{2m} and relative humidity (Leckner, 1978) rather than on GNSS measurements. Previous studies (Nyeki et al., 2005; Morland et al., 2006) concluded that GNSS IWV time series at JFJ are uncertain due to: i) a high variability in IWV values, and ii) the IWV retrieval algorithm is unable to adequately correct for the influence of snow and ice on the GNSS antenna signal.

35   Table 1 also shows cloudiness at each station from APCADA results which have been converted from oktas to FCC. The clearest conditions occur at Locarno (lee location, south of the Alps) with an average FCC value = 0.55 while the cloudiest conditions occur at PAY (plateau location, north of the Alps) with FCC = 0.70 as a result of more persistent stratus cloud cover. Weak seasonal variations are seen to occur at all sites, which are probably associated with synoptic scale weather patterns.

3.2 Surface Radiation Trends and Homogeneity Analysis

To demonstrate the annual cycles in surface radiation at all four stations, DLR time series for all-sky and cloud-free conditions are shown in Figure 1a-d. Maxima in summer and minima in winter are evident as also is the case for DSR (not shown). Lower average DLR values during cloud-free conditions are observed with increasing station altitude (Table 2: 289 W m^{-2} at LOC

5   versus 175 W m^{-2} at JFJ) as reported by Marty et al. (2002) for the same stations. This generally occurs as a result of lower IWV and temperature values with altitude but is not always strictly the case as each station has its own climatology. For instance, the average DLR at PAY in Table 2 is slightly larger than at LOC despite the latter being 124 m lower in altitude. When considering average DSR values with altitude, the situation is similar during cloud-free conditions except that higher long-term averages are generally observed with increasing altitude due to the decrease in atmospheric optical depth. Again,

10   the climatology at each station also has an influence where the cloud-free DSR at LOC (229.3 W m^{-2}) is higher than at PAY and DAV due to lower FCC values (0.51 – 0.58) throughout all seasons.

A summary of the decadal trends (LLS and Sen's slope methods) of all parameters is shown in Table 3. Trend values and confidence levels for both methods are seen to closely agree (i.e. column 3 vs. 4, and 5 vs. 6) in most cases which gives confidence in their use. However, an apparent discrepancy may occur on occasion when time series consist of many outliers

15   or trends are close to zero. In these cases (e.g. JFJ T_{2m} in Table 3) results from the Sen's slope method are preferred as they are considered to be more robust to outliers than the LLS method as well as being more accurate when data are skewed (Wilcox, 2005). In order to be consistent with forerunner studies (Wacker et al., 2011; 2013), results from the LLS method will mainly be discussed here unless otherwise stated. Table 3 also illustrates that trends in T_{2m}, specific humidity and IWV are all positive for all-sky and cloud-free conditions. More specifically, T_{2m}, specific humidity and IWV have increased at all four stations

20   during all-sky and cloud-free conditions on average by ~0.3 – 0.6°C/decade, ~0.1 – 0.2 g kg^{-1}/decade and 0.2 – 0.8 mm/decade, respectively. It is interesting to note that about three quarters of the all-sky and cloud-free trends are significant at the >90% confidence level.

Trends in all-sky and cloud-free DSR are also mainly positive, but few are significant. However, cloud-free trends for PAY and JFJ, at 10.6 and -9.5 W m^{-2}/decade are noticeably larger than for LOC and DAV at 3.3 and 3.1 W m^{-2}/decade, respectively.

25   On closer inspection, the DSR trend at PAY is not monotonic but steeply positive from about the beginning of 2012 to December 2015 whereas the 1996 – December 2011 period exhibits a flat increase of ~2.9 W m^{-2}/decade, which is more comparable to the trends at LOC and DAV. A similar case occurs at JFJ. The trend for 1996 – Dec. 2007 exhibits a flat decrease (~-2.9 W m^{-2}/decade) with a drop for the 2009 – 2015 period. In both cases, homogeneity analysis (described further below) does not suggest that a stepwise change occurred due to a change in instruments etc., so whether these trends continue into the

30   future will have to be further monitored.

Regarding the DLR trends, all are positive and significant at the >90% confidence level except during all-sky conditions at PAY. All-sky DLR trends at the four stations range from 0.9 – 4.3 and 0.9 – 5.9 W m^{-2}/decade for the LLS and Sen's methods, respectively. Larger trends are found for cloud-free conditions with ranges from 2.4 – 5.4 and 2.5 – 5.9 W m^{-2}/decade, respectively, while all trends are significant at the 95% confidence level. The magnitudes and direction of the trends are similar

35   to those observed by Wacker et al. (2011; 2013) with the important exception that DLR time series trends are now significant for virtually all cases (i.e. combinations of stations, cloud conditions, and statistical tests) which was previously observed for only two cases.

Homogeneity analyses of all meteorological and radiation parameters were then conducted to test for any changes in the time series. This is only meaningful when using the full dataset i.e. for all-sky conditions as opposed to cloud-free conditions which

40   are a sub-set of the former. Results from the SNHT, Buishand and Petitt tests indicate that T_{2m} time series from all four stations were homogeneous with significance values of $p > 0.32$, $p > 0.92$ and $p > 0.17$, respectively. Concurrent values for DLR were $p > 0.19$, $p > 0.11$ and $p > 0.15$ while values for other parameters were similar. This suggests that no significant changes in

any of the time series at any station occurred due to climatic or non-climatic effects such as a change of instrument or data acquisition system, relocation, etc.

How do DSR and DLR trends at the four Swiss stations compare to other regions or global averages? In a recent analysis of observed DSR trends at BSRN stations, Wild (2016b) found an overall increase of 2.0 W m^{-2}/decade since the 1990s during

5 all-sky conditions and a similar value cloud-free conditions. The study concluded that a reduction in aerosol concentrations were contributing to the increase in DSR. DLR studies of trends are scarcer. Apart from the earlier mentioned studies (Philipona et al., 2004; Wacker et al., 2011; 2013) which focused on the ASRB network in Switzerland, a global increase of 2.2 W m^{-2}/decade in DLR was estimated for the 1973 – 2008 period (Wang and Liang, 2009) using temperature, humidity and cloud fraction to parameterize DLR. A lower trend of 1.5 W m^{-2}/decade was found in climate model simulations of the Coupled

10 Model Intercomparison Project Phase 5 (CMIP5) by Ma et al. (2014) for the 1979 to 2005 period. In a more recent study by Wild (2016b), 20 of the longest BSRN all-sky DLR time series had an overall average trend of 2.0 W m^{-2}/decade (11 significant) while three were negative (none significant). This agreed well with CMIP5 multi-model mean trends for two RCP scenarios (Representative Concentration Pathways 8.5 and 4.5) which gave all-sky trends of 1.7 and 2.2 W m^{-2}/decade, respectively.

15 **3.3 SCE, LCE and CRE**

3.3.1 Trend Analysis

Time series of the SCE, LCE and CRE were calculated according to Eqs. 1 and 2 after validation of the DSR$_{sim\ cloud-free}$ and DLR$_{sim\ cloud-free}$ parameterizations for the 1996 – 2015 period. Validation was accomplished by determining the shortwave and longwave anomalies (cloud-free – simulated cloud-free values). The mean bias and rmse of the shortwave anomalies were <~9

20 W m^{-2} and <~18 W m^{-2}, respectively, at all four stations while values of -<0.5 W m^{-2} and <~4 W m^{-2} were observed for the longwave anomalies. Our results are similar to those reported by Wacker et al. (2013) for all stations, and in a recent study by Aebi et al. (2017) for DAV and PAY.

The SCE, LCE and CRE time series in Figure 2 are shown for PAY as an example, and illustrate annual variations in each parameter. Values of the long-term averages at all four stations are shown in Table 4 while the trends appear in Table 5.

25 Beginning with a discussion of the SCE, all annual averages are found to be negative with the lowest values (< -70 W m^{-2}) occurring at DAV and PAY. This can be explained by a higher cloud frequency at these sites with FCC = 0.68 and 0.70, respectively, agreeing with short-term results by Aebi et al. (2017). Positive trends of 3.6 – 3.8 W m^{-2}/decade are observed at LOC and PAY which represent a decrease in the magnitude of the SCE. In contrast, SCE trends at DAV and JFJ are close to zero for both LLS and the Sen's slope methods with the latter giving low, negative values (not significant). Apart from the

30 DSR, the SCE depends on the solar zenith angle, IWV and AOD. Figure 3 illustrates the AOD trends at LOC and PAY for the 1996 – 2015 period which are essentially negligible at 0.00 and -0.01 per decade, respectively. Trends at DAV and JFJ are also negligible as shown in a previous study (Nyeki et al., 2012) and in more recent unpublished observations. Increasing DSR and IWV trends at all stations, discussed earlier in section 3.1, are therefore the main reason for an increase in SCE.

Regarding the LCE, annual average values are all positive with the highest occurring at JFJ (49.9 W m^{-2}) and the lowest at

35 LOC (23.3 W m^{-2}), which is partly due to their altitudes at 3580 m and 367 m, respectively. LCE trends are negative at PAY and LOC which are consistent with a decrease in the magnitude of the SCE and the lower all-sky DLR trends with respect to the cloud-free trends at these sites. In contrast, LCE trends at DAV and JFJ are positive, lying in the 1.0 – 2.4 W m^{-2}/decade range but none are significant. Apart from the DLR, the LCE depends on T_{2m}, IWV, the cloud cover and type, and the cloud-base height. In a case study, Aebi et al. (2017) observed that low-level clouds (for example cumulonimbus-nimbostratus or

40 stratus-altostratus) and a cloud coverage of 8 oktas have the highest impact on the magnitude of the LCE with values of 59 – 72 W m^{-2}. The lower the cloud base height, the higher the cloud base temperature and the larger the LCE. It was also shown that there is a negative dependence of the LCE on IWV.

As CRE is the sum of SCE and LCE, its magnitude is smaller during winter due to reduced daylight hours and hence there is a reduced dominance of the SCE. Long-term averages at DAV and PAY therefore have the lowest values at $\sim$ -40 W m^{-2}. Regarding the CRE trends, all are positive and range from 0.9 – 3.1 W m^{-2}/decade, with only the PAY trend significant at the 90% confidence level. While CRE trends in Table 5 are similar to those in Wacker et al. (2013) with a range from 1.3 to 7.4

5 W m^{-2}/decade for 1996 – 2011, SCE and LCE trends are more variable. This can occur when trends are close to zero and when almost none are significant. Table 4 also shows the average values of SCE, LCE and CRE which can be considered as "regional" values for Switzerland. Values of -61.6, 34.1 and -27.6 W m^{-2}, respectively, are comparable to recently updated global average values of -56, 28 and -28 W m^{-2} reported by Wild et al. (2017) using BSRN data.

As a result of the positive CRE trends in Table 5, there is an overall decrease in the CRE magnitude, suggesting that a decrease

10 in fractional cloud cover or a change towards a different cloud type has occurred during the 1996 – 2015 period. This is most likely the case, as any possible changes in AOD, shown further above to be negligible, have already been accounted for in the DSR$_{\text{sim cloud-free}}$ component of CRE. A decrease in cloud cover or a change in cloud type is consistent with the observed increase in the all-sky DSR and reduction in the all-sky DLR trends with respect to their cloud-free counterparts. Despite the observed decrease in CRE, clouds continue to reduce the available radiative energy at the surface over the four SACRaM sites by an

15 overall long-term average of $\sim$ -29 W m^{-2}.

A reduction in cloud cover over Europe and adjoining regions has been ascertained in several studies based on observations and simulations. Sanchez-Lorenzo et al. (2017) reported a decrease in observed and simulated cloud cover during the first two decades of the 1971 – 2005 period over the Mediterranean region which was followed by a subsequent tailing off of the trend. The region of study (30 – 48°N) also covered Switzerland ($\sim$46.2 – 47.6°N) which exhibited a weak, overall decreasing trend

20 in cloud cover. It was argued that the northward expansion of the Hadley cell may be related to the observed changes in cloud cover over the Mediterranean region. In a further recent study based on satellite and BSRN data covering the 1983 – 2015 period, it was concluded that the major part of the overall increasing trend in surface solar radiation over Europe was possibly due to changes in clouds (Pfeifroth et al., 2018).

3.3.2 Trends of Longwave Anomalies

25 Through analysis of the longwave anomaly trends, it is possible to assess the strength of radiative forcing components other than those due to changes in temperature and IWV. Trend analyses are shown in Table 6. The LLS DAV trend of 3.4 W m^{-2}/decade represents 70% of the overall DLR trend of 4.8 W m^{-2}/decade from Table 3. A similarly high value is also found at JFJ, and suggests that 70% of the overall cloud-free trends at these stations are due to factors other than T_{2m} and IWV, as the Prata parameterization only depends on the latter two parameters. In contrast, the trend at LOC (10% value) is almost

30 fully explained by increases in T_{2m} and IWV while PAY (51% value) is partially explained. It is interesting to note that the trends at each station (both LLS and Sen's slope methods) increase with station altitude, although only those at DAV and JFJ are significant.

Previous studies (Philipona et al., 2005; Wacker et al., 2011) have investigated the trends in the longwave anomaly but changes in atmospheric gases or aerosol concentrations were not considered to be the cause. It was noted that the increase

35 in atmospheric CO_2 was responsible for a DLR trend of only $\sim$0.3 W m^{-2}/decade (Prata, 2008) while increases in atmospheric CH_4 and N_2O (Forster et al., 2007) resulted in a trend of $\sim$0.01 W m^{-2}/decade. Furthermore, the effect of aerosols was assumed to be insignificant (Ramanathan et al., 2001). However, it was argued that the use of APCADA, to generate a cloud-free filter, was possibly a biasing factor. As mentioned previously, high-altitude clouds (e.g. cirrus) have a smaller effect on DLR than low or mid-altitude clouds, and hence the cloud-cover filter generated with APCADA may not be accurate during such

40 conditions. If this is the case then a positive trend of the longwave anomaly suggests an increase of the radiative effect of high-level clouds, whereas a negative trend indicates a decrease. Under such assumptions, the positive trends in Table 6 would therefore point to an increase of the radiative effect of high-altitude clouds over the 1996 – 2015 period. The increase in the

trend with station altitude, if real, is more difficult to explain, and may be related to the simple fact that high-altitude stations are closer to high-altitude clouds. As a result, DLR could be enhanced. However, a possible change in the radiative effect of high-altitude clouds remains to be determined in detail with other techniques.

3.3.3 Improvement of Methods

As mentioned earlier in Section 2.3, the DLR-IWV parameterization was investigated as an alternative to the modified Prata parameterization to determine $DLR_{sim\,cloud-free}$. Figure 4 shows monthly average values of observed DLR versus IWV during all-sky and cloud-free conditions for the 2000 – 2015 period. DLR is seen to be less sensitive to changes in IWV at higher IWV values, which is due to saturation of longwave absorption in the atmospheric longwave window. The power-law fits (black curves) in both graphs have been calculated for ≥679 monthly average values, and agree well with superimposed curves (red) from Ruckstuhl et al. (2007) for the 2001 – 2004 period. Fits for all-sky and cloud-free conditions exhibit values $R^2 = 0.95$ and 0.97 with rmse = 10.0 and 10.1 W m^{-2}, respectively. Despite the good overall fit, Figure 4 shows that the agreement becomes poorer when IWV ≲ 5 mm, especially during cloud-free conditions. These are mainly JFJ data points which have a high uncertainty due to the aspects discussed earlier in section 3.1. The greater scatter in both graphs with respect to that of the modified Prata parameterization (rmse < 4.0 W m^{-2}, all stations) therefore suggests that this straightforward parameterization of cloud-free DLR using only IWV will not allow sufficiently accurate LCE trends to be determined, even with longer time series.

A promising alternative to APCADA to determine the degree of cloud cover is the use of sky cameras. As only the 2013 – 2015 FCC time series at DAV and PAY were available for the present study, it was tried on the above DLR-IWV parameterization. Rmse values of 13.7 W m^{-2} and 12.8 W m^{-2} were obtained for all-sky ($R^2 = 0.80$) and cloud-free conditions ($R^2 = 0.85$), respectively. These values are higher than with APCADA (10.0 and 10.1 W m^{-2}) but are likely to improve (i.e. decrease) when longer time series become available in the future. A further refinement is the use of an infrared sky camera which allows cloud cover to be determined during the night. A research prototype, the thermal infrared cloud camera (IRCCAM), has been continuously operating at DAV since September 2015 (Aebi et al., 2018). A comparison of IRCCAM with the visible sky cameras gave FCC values to within ±0.07 and to within ±0.05 for APCADA. Aebi et al. (2018) concluded that the use of FCC from infrared sky cameras could increase the accuracy of cloud-free climatologies when FCC time series of adequate length become available.

4 Conclusions

The trends of surface downward shortwave and longwave radiation (DSR, DLR) were analyzed at four stations (between 370 and 3580 m asl) in Switzerland for the 1996 – 2015 period. Using these data and meteorological parameters, the cloud radiative effect (CRE) was determined from calculations of the shortwave and longwave cloud radiative effects. The main conclusions include the following:

1) Trends in ground temperature, specific humidity and IWV all increased during all-sky and cloud-free conditions. A large number were significant at the ≥90% confidence level.

2) All-sky and cloud-free DSR trends were in the ranges 0.6 – 4.3 W m^{-2}/decade and -2.9 – 3.3 W m^{-2}/decade, respectively. A large number of trends were significant at the ≥90% confidence level.

3) All-sky and cloud-free DLR trends were all positive and in the ranges 0.9 – 4.3 W m^{-2}/decade and 2.9 – 5.4 W m^{-2}/decade, respectively. All but one trend was significant at the ≥90% confidence level.

4) The net radiative cooling due to clouds, the CRE, decreased in magnitude by 0.9 – 3.1 W m^{-2}/decade over the 1996 – 2015 period, which implies a decrease in cloud cover or a change towards a different cloud type.

5) Between 10 and 70% of the increase in DLR is explained by factors other than T_{2m} and IWV. An increase in cloud cover by high level clouds is consistent with these observations. However, it is not possible to quantify or verify changes in cloud properties in further detail as cloud cameras, ceilometers, lidar, etc. have only been installed to varying degrees at the four SACRaM stations in recent years.

5 6) Trends in AOD at each station during the 1996 – 2015 period were insignificant, and hence their impact on the observed surface radiative fluxes was negligible.

Although accurate DSR and DLR time-series have been available for more than 20 years in Switzerland, the detection of trends with high confidence remains difficult due to the relatively small changes in surface radiation and cloud properties which are

10 close to the measurement uncertainty. Therefore, it is crucial to continue providing facilities to maintain such radiation observations of the highest possible accuracy which allow, despite their simplicity, changes in radiation and clouds to be reliably assessed. A reduction in quality, data gaps or discontinuation of these observations may hamper the accurate detection of any trend, and thus hamper climate monitoring. Regarding the observations of clouds, it is essential to apply and develop methods which can be used during night and day to detect clouds reliably. In addition, these methods should be capable of

15 determining cloud properties, i.e. cloud type in order to verify hypotheses from observed radiation data. Such methods include lidar and cloud radar which are limited, however, to a few super-sites due their high costs. Alternatively, visible and infrared sky cameras are promising methods which would allow basic cloud properties to be monitored on a more widespread basis.

Data availability. The data sets analysed in this study are available from the corresponding author upon request
20 (stephan.nyeki@pmodwrc.ch).

Author contributions. SW and JG designed the study. LV provided measurement data. SN performed the data analysis, interpreted the results and wrote the manuscript with help from SW. All other co-authors contributed by commenting and revising the paper.

25

Acknowledgments. The author was kindly financed through the Swiss GAW CRUX project by MeteoSwiss. IWV data were taken from the STARTWAVE database which is managed by the Institute of Applied Physics, University of Bern.

References

Ackerman, T. P., and Stokes, G. M.: The atmospheric radiation measurement program, Physics Today, 56, 38-44, 2003.

30 Aebi, C., Gröbner, J., Kämpfer, N., and Vuilleumier, L.: Cloud radiative effect, cloud fraction and cloud type at two stations in Switzerland using hemispherical sky cameras, Atmos. Meas. Technol., 10, 4587-4600, doi:10.5194/amt-10-4587-2017, 2017.

Aebi, C., Gröbner, J., and Kämpfer, N.: Cloud fraction determined by thermal infrared and visible all-sky cameras, Atmos. Meas. Tech., 11, 5549-5563, https://doi.org/10.5194/amt-11-5549-2018, 2018.

35 Augustine, J. A., DeLuisi, J. J., and Long, C. N.: SURFRAD – a national surface radiation budget network for atmospheric research, Bulletin of the American Meteorological Society, 81, 2341-2357, 2000.

Berg, L. K., Kassianov, E. I., Long, C. N., and Mills Jr., D. L.: Surface summertime radiative forcing by shallow cumuli at the Atmospheric Radiation Measurement Southern Great Plains site, J. Geophys. Res., 116, D01202, doi:10.1029/2010JD014593, 2011.

40 Brutsaert, W.: On a derivable formula for long-wave radiation from clear skies, Water Resource and Research, 11, 742-744, doi:10.1029/WR011i005p00742, 1975.

Dürr, B.: The greenhouse effect in the Alps by models and observations, Ph.D. thesis, 81 pp., Swiss Fed. Inst. of Technol. at Zurich, Zurich, Switzerland, 2004.

Dürr, B., and Philipona, R.: Automatic cloud amount detection by surface longwave downward radiation measurements, J. Geophys. Res., 109, D05201, doi:10.1029/2003JD004182, 2004.

5 Fehlmann, A., Kopp, G., Schmutz, W., Winkler, R., Finsterle, W., and Fox, N.: Fourth World Radiometric Reference to SI radiometric scale comparison and implications for on-orbit measurements of the total solar irradiance, Metrologia, 49, S34-S38, doi:10.1088/0026-1394/49/2/S34, 2012.

Forster, P., et al.: Changes in atmospheric constituents and in radiative forcing, in Climate Change 2007: The Physical Science Basis, edited by S. Solomon et al., pp. 137-141, Cambridge Univ. Press, Cambridge, UK, 2007.

10 Gilbert, R.: Statistical Methods for Environmental Pollution Monitoring, Van Nostrand Reinhold, New York. 1987.

Gröbner, J., Wacker, S., Vuilleumier, L., and Kämpfer, N.: Effective atmospheric boundary layer temperature from longwave radiation measurements, J. Geophys. Res., 114, D19116, doi:10.1029/2009JD012274, 2009.

Gröbner, J., Reda, I., Wacker, S., Nyeki, S., Behrens, K., and Gorman, J.: A new absolute reference for atmospheric longwave irradiance measurements with traceability to SI units, J. Geophys. Res., 119, doi:10.1002/2014JD021630, 2014.

15 Gröbner, J. et al.: The 2nd International Pyrgeometer Intercomparison, IPgC-II, WMO IOM Report, No. 129, 2018.

Gubler, S, Gruber, S., and Purves, R. S.: Uncertainties of parameterized surface downward clear-sky shortwave and all-sky longwave radiation, Atmos. Chem. Phys., 12, 5077-5098, doi:10.5194/acps-12-5077-2012, 2012.

Kazadzis, S., Kouremeti, N., Nyeki, S., Gröbner, J., and Wehrli, C.: The World Optical Depth Research and Calibration Center (WORCC) quality assurance and quality control of GAW-PFR AOD measurements, Geoscientific Instrumentation,

20 Methods and Data Systems, 7, 39–53, doi:10.5194/gi-7-39-2018, 2018.

König-Langlo, G., Sieger, R., Schmithüsen, H., Bücker, A., Richter, F., Dutton, E. G.: The baseline surface radiation network and its world radiation monitoring centre at the Alfred Wegener Institute, GCOS Report 174: update of the technical plan for BSRN data management. World Meteorological Organization (WMO), www.wmo.int/pages/prog/gcos/Publications/gcos-174.pdf, 2013.

25 Leckner, B.: The spectral distribution of solar radiation at the Earth's surface - elements of a model, Solar Energy, 20 (2), 1978.

Long, C. N., and Turner, D. D.: A method for continuous estimation of clear-sky downwelling longwave radiative flux developed using ARM surface measurements, J. Geophys. Res., 113, D18206, doi:10.1029/2008JD009936, 2008.

Ma, Q., Wang, K. C., and Wild, M.: Evaluations of atmospheric downward longwave radiation from 44 coupled general

30 circulation models of CMIP5, J. Geophys. Res., 119, 4486-4497, doi:10.1002/2013JD021427, 2014.

Marty, C.: Surface radiation, cloud forcing and greenhouse effect in the Alps, Ph.D. thesis, 122 pp., Swiss Fed. Inst. of Technol. at Zurich, Zurich, Switzerland, 2000.

Marty, C., Philipona, R., Fröhlich, C., and Ohmura, A.: Altitude dependence of surface radiation fluxes and cloud forcing in the Alps: Results from the alpine surface radiation budget network, Theoretical and Applied Climatology, 72, 137-154,

35 2002.

Mayer, B., and Kylling, A.: Technical note: The libRadtran software package for radiative transfer calculations - description and examples of use, Atmospheric Chemistry and Physics, 5, 1855-1877, doi:10.5194/acp-5-1855-2005, 2005.

McFarlane, S., Long, C. N., and Flaherty, J.: A climatology of surface cloud radiative effects at the ARM tropical western Pacific sites, Journal of Applied Meteorology and Climatology, 52, 996-1031, doi:10.1175/JAMC-D-0189.1, 2012.

40 Meloni, D., Di Biagio, C., Di Sarra, A., Monteleone, F., Pace, G., and Sferlazzo, D. M.: Accounting for the solar radiation influence on downward longwave irradiance measurements by pyrgeometers, Journal of Atmospheric and Oceanic Technology, 29, 1629-s1643, doi:10.1175/JTECH-D-11-00216.1, 2012.

Morland, J., Liniger, M. A., Kunz, H., Balin, I., Nyeki, S., Mätzler, C., and Kämpfer, N.: Comparison of GPS and ERA40 IWV in the Alpine region, including correction of GPS observations at Jungfraujoch (3584 m), J. Geophys. Res., 111, D04102, doi:10.1029/2005JD006043, 2006.

Nyeki, S., Vuilleumier, L., Morland, J., Bokoye, A., Viatte, P., Mätzler, C., and Kämpfer, N.: A 10-year integrated atmospheric
5   water vapor record using precision filter radiometers at two high-alpine sites, Geophysical Research Letters, 32, L23803, doi:10.1029/2005GL024079, 2005.

Nyeki, S., Halios, C. H., Baum, W., Eleftheriadis, K., Flentje, H., Gröbner, J., Vuilleumier, L., and Wehrli, C.: Ground-based aerosol optical depth trends at three high-altitude sites in Switzerland and southern Germany from 1995 to 2010, J. Geophys. Res., 117, D18202, doi:10.1029/2012JD017493, 2012.

10 Nyeki S., Wacker, S., Gröbner, J., Finsterle, W., and Wild, M.: Revising short and longwave radiation archives in view of possible revisions of the WSG and WISG reference scales: Methods and implications, Atmos. Meas. Technol., 10, 3057-3071, doi:10.5194/amt-10-3057-2017, 2017.

Ohmura, A., Dutton, E. G., Forgan, B., Fröhlich, C., Gilgen, H., Hegner, H., Heimo, A., König-Langlo, G., McArthur, B., Müller, G., Philipona, R., Pinker, R., Whitlock, C. H., Dehne, K., and Wild, M.: Baseline surface radiation network
15 (BSRN/WRCP): New precision radiometry for climate research, Bulletin of the American Meteorological Society, 79, 2115-2136, 1998.

Philipona, R., Marty, C., and Fröhlich, C.: Measurements of the long-wave radiation budget in the Alps, in IRS 96: Current Problems in Atmospheric Radiation, pp. 786–789, A. Deepak, Hampton, Va., 1996.

Philipona, R., Dürr, B., Marty, C., Ohmura, A., and Wild, M.: Radiative forcing - measured at Earth's surface corroborate the
20   increasing greenhouse effect, Geophysical Research Letters, 31, L03202, doi:10.1029/ 2003GL018765, 2004.

Philipona, R., Dürr, B., Ohmura, A., and Ruckstuhl, C.: Anthropogenic greenhouse forcing and strong water vapor feedback increase temperature in Europe, Geophysical. Research Letters, 32, L19809, doi:10.1029/2005GL023624, 2005.

Pfeifroth, U., Sanchez-Lorenzo, A., Manara, V., Trentmann, J., and Hollmann, R.: Trends and variability of surface solar radiation in Europe based on surface- and satellite-based data records, J. Geophys. Res., 123, 1735-1754,
25   doi:10.1002/2017JD027418, 2018.

Prata, A. J.: A new long-wave formula for estimating downward clear-sky radiation at the surface, Quarterly Journal of the Royal Meteorological Society, 122, 1127-1151, 1996.

Prata, R.: The climatological record of clear-sky longwave radiation at the Earth's surface: evidence for water vapour feedback? Journal of Remote Sensing, 29, 5247-5263, doi:10.1080/01431160802036508, 2008.

30 Ramanathan, V., Cess, R., Harrison, E., Minnis, P., Barkstrom, P., Ahmad, A., and Hartmann, D.: Cloud-radiative forcing and climate: Results from the Earth Radiation Budget Experiment, Science, 243, 57-63, 1989.

Ramanathan, V., Crutzen, P. J., Kiehl, J. T., and Rosenfeld, D.: Aerosols, climate, and the hydrological cycle, Science, 294, 2119-2124, 2001.

Roesch, A., Wild, M., Ohmura, A., Dutton, E.G., Long, C. N., and Zhang, T.: Assessment of BSRN radiation records for the
35   computation of monthly means, Atmospheric Measurement and Technology 4(2), 339-354, doi:10.5194/amt-4-339-2011, 2011.

Ruckstuhl, C., Philipona, R., Morland, J., and Ohmura, A.: Observed relationship between surface specific humidity, integrated water vapor, and longwave downward radiation at different altitudes, J. Geophys. Res., 112, D03302, doi:10.1029/2006JD007850, 2007.

40 Sanchez-Lorenzo, A., Enriquez-Alonso, A., Calbo, J., Gonzalez, J-A., Wild, M., Folini, D., Norris, J. R., and Vicente-Serrano, S. M.: Fewer clouds in the Mediterranean: consistency of observations and climate simulations, Scientific Reports, 7, 41475, doi:10.1038/srep41475, 2017.

Vuilleumier, L., Hauser, M., Félix, C., Vignola, F., Blanc, P., Kazantzidis, A., and Calpini B.: Accuracy of ground surface broadband shortwave radiation monitoring, J. Geophys. Res., 119, doi:10.1002/2014JD022335, 2014.

Wacker, S., Gröbner, J., Hocke, K., Kämpfer, N., and Vuilleumier L.: Trend analysis of surface clear-sky downwelling long-wave radiation from four Swiss sites, J. Geophys. Res., 116, D10104, doi:10.1029/2010JD015343, 2011.

Wacker, S., Gröbner, J., and Vuilleumier L.: Trends in surface radiation and cloud radiative effect over Switzerland in the past 15 years, AIP Conference Proceedings, 1531, 672, doi:101063.1.4804859, 2013.

Wacker, S., Gröbner, J., and Vuilleumier L.: A method to calculate cloud-free long-wave irradiance at the surface based on radiative transfer modeling and temperature lapse rate estimates, Theoretical and Applied Climatology, 115, doi:10.1007/s00704-013-0901-5, 2014.

Wacker, S., Gröbner, J., Zysset, C., Diener, L., Tzoumanikas, P., Kazantzidis, A., Vuilleumier, L., Stöckli, R., Nyeki, S., and Kämpfer N.: Cloud observations in Switzerland using hemispherical sky cameras, J. Geophys. Res., 120, doi:10.1002/2014JD022643, 2015.

Wang, K. C, and Liang, S. L.: Global atmospheric downward longwave radiation over land surface under all-sky conditions from 1973 to 2008, J. Geophys. Res. 114, D19101, 2009.

Wang, K., and Dickinson, R. E.: Global atmospheric downward longwave radiation at the surface from ground-based observations, satellite retrievals, and reanalyses, Reviews of Geophysics, 150-185, 51, 2013.

Weatherhead, E. C., Reinsel, G. C., Tiao, G. C., Meng, X.-Li, Choi, D., Cheang, W.-K., Keller, T., DeLuisi, J., Wuebbles, D. J., Kerr, J. B., J. Miller, A., Oltmans, S. J., and Frederick, J. E.: Factors affecting the detection of trends: Statistical consideration and applications to environmental data, J. Geophys. Res., 103 (D14), 17,149-17,161, doi:10.1029/98JD00995, 1998.

Wijngaard, J. B., Klein Tank, A. M. G., and Können G. P.: Homogeneity of 20th century European daily temperature and precipitation series, International Journal of Climatology, 23, 679-692, doi:10.1002/joc.906, 2003.

Wilcox, R. R.: Theil-Sen Estimator, in Introduction to Robust Estimation and Hypothesis Testing, Academic Press, pp. 423-427. ISBN 978-0-12-751542-7, 2005.

Wild, M.: Global dimming and brightening: A review, J. Geophys. Res., 114, D00D16, doi:10.1029/2008JD011470, 2009.

Wild, M.: Decadal changes in radiative fluxes at land and ocean surfaces and their relevance for global warming, WIREs Climate Change, 7, 91-107, doi:10.1002/wcc.372, 2016a.

Wild, M.: Changes in shortwave and longwave radiative fluxes as observed at BSRN sites and simulated with CMIP5 models, AIP Conference Proceedings, 1810, 090014-1, doi:10.1063/1.4975554, 2016b.

Wild, M., Hakuba, M. Z., Folini, D., Schär, C., and Long, C.: New estimates of the Earth radiation budget under cloud-free conditions and cloud radiative effects, AIP Conference Proceedings, 1810, 090012 (2017), doi:10.1063/1.4975552, 2017.

WMO: CIMO-XIV, Activity Report, 7–14 December 2006, WMO No. 1019 (Part II), 2006.

Table 1: Summary of selected parameters during all-sky conditions for the 1996 – 2015 period at the four indicated stations (ordered by ascending altitude). Average values constructed from 10-min data are shown with the standard deviations in brackets.

Parameter	Station	Spring (MAM)	Summer (JJA)	Fall (SON)	Winter (DJF)	Annual
Temperature, T_{2m}	LOC (367 m)	12.8 (5.4)	21.3 (4.2)	12.8 (5.3)	4.3 (3.5)	12.8 (7.6)
(°C)	PAY (491 m)	9.6 (6.0)	18.3 (5.1)	9.8 (5.8)	1.2 (4.4)	9.8 (8.1)
	DAV (1594 m)	3.3 (6.2)	12.0 (5.1)	4.6 (6.2)	−4.3 (5.1)	4.0 (8.1)
	JFJ (3580 m)	-8.6 (5.1)	-0.3 (3.7)	-5.4 (5.4)	-12.6 (5.2)	-6.7 (6.6)
Specific humidity	LOC	5.6 (2.3)	10.3 (2.5)	7.0 (2.6)	3.4 (1.2)	6.6 (3.3)
(g kg^{-1})	PAY	5.7 (1.9)	9.6 (1.9)	6.8 (2.2)	3.7 (1.1)	6.5 (2.8)
	DAV	4.1 (1.4)	7.5 (1.6)	5.0 (1.8)	2.6 (1.0)	4.8 (2.3)
	JFJ	2.3 (1.2)	4.3 (1.5)	2.7 (1.4)	1.5 (0.8)	2.7 (1.6)
IWV	LOC	15.8 (6.2)	28.0 (7.3)	19.0 (7.2)	10.0 (4.1)	18.1 (9.0)
(mm)	PAY	14.4 (5.4)	24.4 (6.1)	17.3 (6.3)	10.0 (4.2)	16.4 (7.6)
	DAV	9.5 (3.6)	17.0 (4.1)	11.3 (4.3)	6.4 (2.8)	11.0 (5.4)
	JFJ*	4.6 (2.2)	8.3 (2.8)	5.3 (2.7)	3.0 (1.5)	5.3 (3.0)
DSR	LOC	191.2 (275.7)	249.0 (317.1)	111.0 (193.1)	72.0 (134.1)	156.2 (250.8)
(W m^{-2})	PAY	184.7 (261.6)	242.7 (304.5)	100.5 (176.5)	53.7 (106.5)	145.7 (237.5)
	DAV	204.0 (283.4)	229.8 (309.6)	119.3 (199.6)	78.0 (142.0)	158.4 (251.3)
	JFJ	235,6 (311.4)	265.9 (338.7)	140.4 (224.7)	84.9 (153.5)	182.4 (277.5)
DLR	LOC	310.5 (39.5)	360.6 (29.7)	320.7 (42.0)	269.6 (37.1)	315.6 (49.4)
(W m^{-2})	PAY	304.5 (38.6)	348.0 (30.1)	318.2 (37.4)	285.2 (37.6)	314.1 (42.7)
	DAV	276.4 (39.9)	319.6 (30.2)	282.7 (40.2)	243.5 (41.6)	280.4 (46.9)
	JFJ	224.6 (50.8)	260.9 (45.5)	231.1 (49.8)	201.1 (50.3)	229.4 (53.5)
Fractional cloud	LOC	0.56	0.54	0.58	0.51	0.55
Cover, FCC	PAY	0.64	0.60	0.74	0.81	0.70
	DAV	0.70	0.72	0.66	0.64	0.68
	JFJ	0.70	0.74	0.64	0.61	0.67

*IWV at JFJ based on parameterization (Leckner, 1978) rather than GNSS measurements. See text for discussion.

Table 2: Similar to Table 1 except for cloud-free conditions.

Parameter	Station	Spring (MAM)	Summer (JJA)	Fall (SON)	Winter (DJF)	Annual
Temperature, T_{2m}	LOC	13.9 (5.7)	22.6 (4.3)	13.5 (5.9)	4.9 (4.0)	13.6 (8.1)
(°C)	PAY	10.1 (7.1)	19.5 (5.8)	10.9 (6.6)	0.4 (4.9)	11.9 (8.9)
	DAV	3.4 (7.1)	13.5 (5.6)	5.3 (6.8)	−5.1 (5.6)	3.8 (9.1)
	JFJ	-7.9 (5.1)	1.0 (3.5)	-3.9 (5.4)	-11.3 (5.0)	-6.0 (6.6)
Specific humidity	LOC	4.7 (2.1)	9.6 (2.6)	6.2 (2.6)	2.9 (1.0)	5.9 (3.3)
(g kg^{-1})	PAY	5.3 (1.9)	9.5 (2.0)	6.9 (2.3)	3.3 (0.9)	6.8 (2.9)
	DAV	3.5 (1.3)	7.2 (1.5)	4.6 (1.7)	2.1 (0.8)	4.2 (2.3)
	JFJ	1.7 (1.0)	3.4 (1.5)	2.0 (1.2)	1.1 (0.6)	2.0 (1.3)
IWV	LOC	12.7 (5.5)	25.0 (7.0)	15.6 (6.4)	7.9 (3.1)	15.1 (8.5)
(mm)	PAY	12.0 4.8)	22.1 (5.4)	15.3 (5.4)	7.7 (3.2)	15.3 (7.2)
	DAV	7.4 (3.1)	15.3 (3.6)	9.2 (3.6)	4.5 (2.0)	8.8 (4.9)
	JFJ*	3.3 (1.8)	6.5 (2.8)	4.0 (2.2)	2.2 (1.3)	3.8 (2.5)
DSR	LOC	270.2 (320.1)	358.9 (356.3)	177.1 (238.4)	99.6 (159.8)	229.3 (295.7)
(W m^{-2})	PAY	257.7 (313.4)	328.3 (347.0)	166.2 (237.3)	99.7 (160.5)	206.8 (304.3)
	DAV	265.9 (336.2)	309.4 (362.2)	176.1 (246.0)	109.4 (176.5)	216.2 (294.2)
	JFJ	299.5 (388.7)	354.7 (408.4)	190.3 (270.2)	116.6 (187.0)	244.9 (328.1)
DLR	LOC	283.1 (31.3)	344.1 (26.7)	290.1 (33.3)	241.9 (17.9)	289.3 (46.3)
(W m^{-2})	PAY	274.8 (31.3)	329.9 (26.6)	286.7 (32.1)	234.0 (19.9)	289.6 (43.5)
	DAV	237.5 (28.2)	291.5 (22.2)	249.4 (28.2)	204.5 (20.6)	243.4 (39.8)
	JFJ	167.6 (22.3)	207.9 (18.0)	182.3 (23.6)	151.9 (19.4)	175.2 (29.1)

*IWV at JFJ based on parameterization (Leckner, 1978) rather than GNSS measurements. See text for discussion.

Table 3: Trend analyses (linear least squares, LLS, and Sen's methods) of selected parameters for the 1996 – 2015 period during all-sky and cloud-free conditions at all four stations. Trend values in italic (bold) are significant at the 90% (95%) level. The upper and lower bounds of the 90% confidence interval for the DLR trends are shown in Figure 1 as an example but have been omitted here and in other tables for clarity.

Parameter	Station	All-sky LLS method slope/decade	All-sky Sen's slope slope/decade	Cloud-free LLS method slope/decade	Cloud-free Sen's slope slope/decade
Temperature, T_{2m}	LOC	**0.43**	**0.53**	**0.54**	**0.66**
(°C)	PAY	*0.35*	**0.50**	**0.59**	**0.79**
	DAV	0.30	0.44	*0.48*	**0.61**
	JFJ	0.34	0.43	0.20	0.16
Specific humidity	LOC	**0.19**	**0.18**	0.14	0.12
(g kg^{-1})	PAY	**0.18**	**0.19**	**0.23**	**0.18**
	DAV	*0.08*	0.08	*0.10*	0.10
	JFJ	**0.14**	**0.14**	**0.19**	**0.19**
IWV	LOC	0.37	0.42	0.36	0.31
(mm)	PAY	0.41	**0.80**	*0.58*	**1.03**
	DAV	**0.63**	**0.89**	**0.79**	**1.18**
	JFJ*	**0.24**	**0.26**	**0.27**	**0.25**
DSR	LOC	*4.3*	**5.5**	3.3	**3.8**
(W m^{-2})	PAY	*3.4*	*3.4*	**10.6****	**10.0****
	DAV	0.6	0.2	3.1	3.5
	JFJ	*3.6*	2.2	**-9.5*****	**-10.3*****
DLR	LOC	*2.5*	*2.5*	**2.9**	**3.2**
(W m^{-2})	PAY	0.9	0.9	**2.4**	*2.5*
	DAV	**2.7**	**3.2**	**4.8**	**5.8**
	JFJ	**4.3**	**5.9**	**5.4**	**5.9**

*IWV at JFJ based on parameterization (Leckner, 1978) rather than GNSS measurements. See text for discussion. **Trends for 1996 – Dec. 2011 are 2.9 and 3.0 W m^{-2}/decade (none significant) for the LLS and Sen's methods, respectively. ***Trends for 1996 – Dec. 2007 are -2.9 and -1.7 W m^{-2}/decade (none significant), respectively.

5 **Table 4: Long-term average values of the shortwave and longwave cloud effects (SCE and LCE, respectively), and cloud radiative effect (CRE) for the 1996 – 2015 period at all four stations. The one sigma uncertainty is shown in brackets.**

Station	SCE (W m^{-2})	LCE (W m^{-2})	CRE (W m^{-2})
LOC	-47.7 (±6.1)	23.3 (±2.8)	-24.4 (±5.1)
PAY	-71.9 (±5.5)	31.1 (±2.5)	-40.8 (±4.4)
DAV	-72.8 (±5.6)	32.1 (±3.0)	-40.7 (±3.9)
JFJ	-54.2 (±3.9)	49.9 (±5.6)	-4.3 (±5.3)
Average	-61.6 (±7.4)	34.1 (±3.7)	-27.6 (±5.4)

Table 5: Trend analysis of the shortwave and longwave cloud effects (SCE and LCE), and cloud radiative effect (CRE) for the 1996 – 2015 period at all four stations. Trends in italic (bold) are significant at the 90% (95%) confidence level.

Station	SCE (W m^{-2}/decade)		LCE (W m^{-2}/decade)		CRE (W m^{-2}/decade)	
	LLS	Sen's Slope	LLS	Sen's Slope	LLS	Sen's Slope
LOC	3.6	2.2	-0.7	-0.5	2.9	2.3
PAY	*3.8*	*3.8*	-0.6	-0.9	*3.1*	*2.3*
DAV	-0.1	-0.4	1.0	1.4	0.9	1.3
JFJ	0.1	-0.5	2.4	2.8	2.5	2.4

Table 6: Trend analysis of the longwave anomalies during cloud-free conditions for the 1996 – 2015 period at all four stations. Trend values in italic (bold) are significant at the 90% (95%) level. Percentage values in brackets correspond to the contribution of the anomaly to the overall trends in Table 3.

Station	Longwave	
	LLS method (W m^{-2}/decade)	Sen's slope (W m^{-2}/decade)
LOC	0.3 (10%)	0.3 (9%)
PAY	1.2 (51%)	1.3 (46%)
DAV	**3.4 (70%)**	**3.1 (60%)**
JFJ	**3.8 (70%)**	**4.6 (78%)**
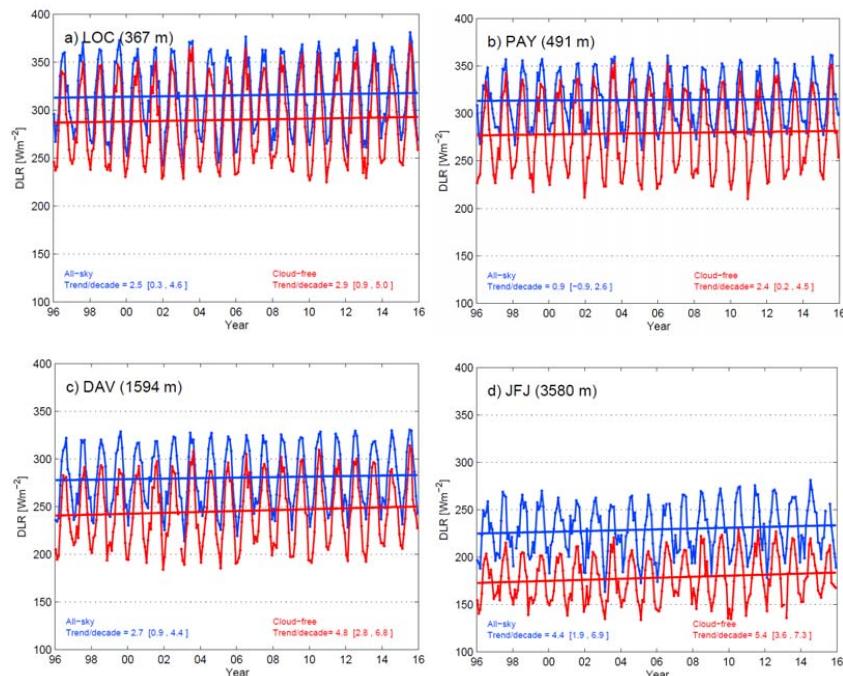
Figure 1: Monthly average DLR values during all-sky (blue) and cloud-free (red) conditions at: a) Locarno, b) Payerne, c) Davos, and d) Jungfraujoch. Each panel also shows trend results from linear least squares analysis using the Weatherhead et al. (1998) method. Values in brackets represent the upper and lower bounds of the 90% confidence interval. Scales are similar to aid the comparison.

25

30

35

40
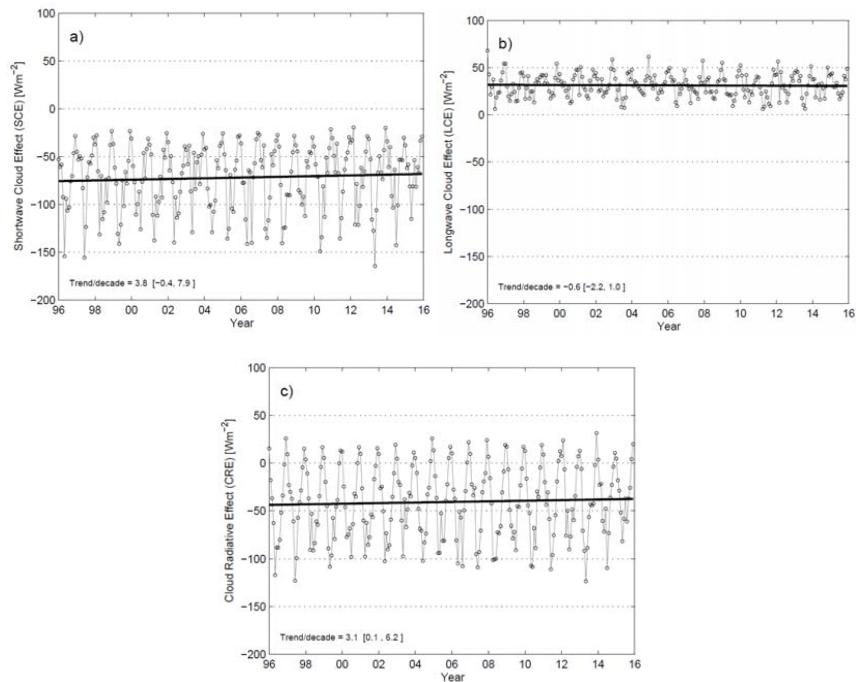
Figure 2: Time series of monthly average: a) SCE, b) LCE and c) CRE values at Payerne (PAY). Values in brackets represent the upper and lower bounds of the 90% confidence interval.

25

30

35

40

45
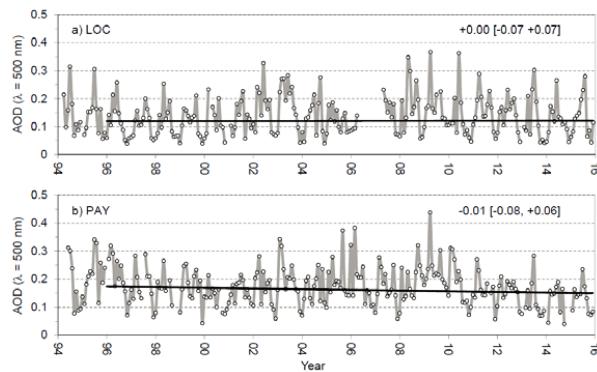
Figure 3: Time series of monthly AOD (= 500 nm) averages available since 1994 at: a) LOC and b) PAY. The 1996 – 2015 decadal trend is shown in the top right-hand corner where values in brackets represent the upper and lower bounds of the 90% confidence interval. Trend values are only shown for the 1996 – 2015 period to be consistent with other trend periods in this study.

25
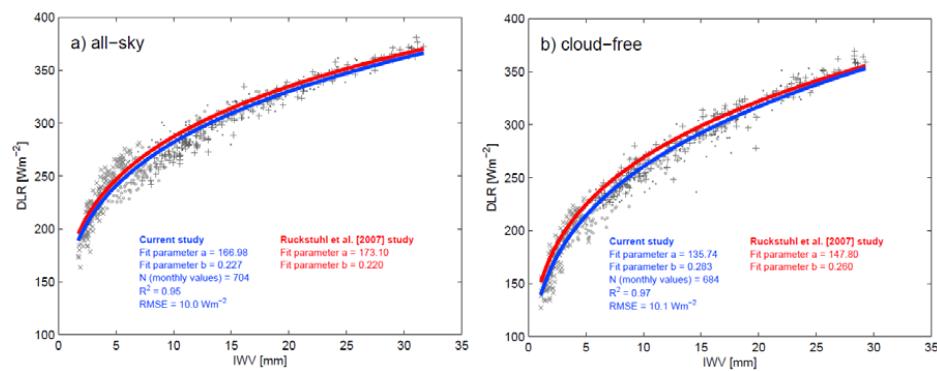
Figure 4: Monthly average DLR at all four stations (symbols: LOC = plus symbols, PAY = closed circles, DAV = open circles, and JFJ = crosses) for the 1996 – 2015 period versus IWV values during: a) all-sky conditions, and b) cloud-free conditions.